Change Detection in Wavelength-Resolution SAR Image Stack Based on Tensor Robust PCA

Lucas P. Ramos, *Graduate Student Member, IEEE*, Dimas I. Alves, *Member, IEEE*, Leonardo T. Duarte, *Senior Member, IEEE*, Renato Machado, *Senior Member, IEEE*, Mats I. Pettersson, *Senior Member, IEEE*, Viet T. Vu, and Patrik Dammert, *Senior Member, IEEE*

***Abstract*— Wavelength-resolution (WR) synthetic aperture radar (SAR) change detection (CD) has been used to detect concealed targets in forestry areas. However, most proposed methods are generally based on matrix or vector analyses and, therefore, do not exploit information embedded in multidimensional data. In this letter, a CD method for WR SAR image stacks based on tensor robust principal component analysis (TRPCA) is proposed. The proposed CD method used the new tensor nuclear norm (TNN) induced by the definition of the tensor–tensor product to exploit temporal and spatial information contained in the image stack. To assess the performance of the proposed method, we considered SAR images obtained by the very high-frequency (VHF) WR coherent all radio band sensing (CARABAS)-II SAR system. Experiments for three different stack sizes show that a significant performance gain can be achieved when large image stacks are considered. The proposed CD method performs better in terms of probability of detection (PD) and false alarm rate (FAR) than the other five CD methods in VHF WR SAR images, including one based on matrix robust principal component analysis (RPCA). In a particular setting, it achieves a PD of 99% and an FAR of 0.028 false alarms (FAs) per km^2.**

***Index Terms*— Change detection (CD), coherent all radio band sensing (CARABAS)-II, synthetic aperture radar (SAR), tensor robust PCA.**

I. Introduction

DETECTING changes in remote sensing images of the same scene taken at different times is of great interest, as it allows dynamically processing satellite maps, observing environmental changes, and monitoring land use and land cover [1], [2]. Synthetic aperture radar (SAR) images are acquired by active microwave sensors and have proven to be an ideal source for change detection (CD) applications because they can monitor the Earth independently of sunlight conditions and cloud coverage [3].

It is understood that the design of the SAR system depends on the application of interest. Wavelength-resolution (WR) SAR systems have been used targeting different applications such as high-resolution imaging, ground-moving target indication, and CD [4]. WR SAR systems are characterized by a large fractional bandwidth, e.g., ultrawideband (UWB) and a wide antenna bandwidth [5]. In these systems, the scattering process is related to scatters with dimensions in the order of the signal wavelengths [6]. Thus, the resolution cell contains only a single scatter, and consequently, SAR images generated by WR SAR systems do not suffer from speckle noise. When operating in frequency bands below 1 GHz, for instance, the one used in this article, i.e., very high frequency (VHF), the main contribution to the clutter comes from large static objects generally stable in time and less sensitive to weather conditions. Then, measurements performed by VHF WR SAR systems become stable across different acquisitions [7].

The first CD methods for this type of SAR image were based on pairs of images, i.e., an interest image that changes are expected to have occurred and a reference image [8], [9]. However, other studies showed that using small stacks of SAR images improves the performance of the CD method [10], [11]. For example, Ramos et al. [12] proposed a CD method based on robust principal component analysis (RPCA) via principal component pursuit (PCP) [13] for WR SAR image stacks, extending the work proposed in Schwartz et al. [14], which was proposed for SAR image pairs and validating that this increase in information contributes to a performance gain by reducing the number of false alarms (FAs). RPCA method pursues a decomposition of the input SAR data into a low-rank, which seeks to model the clutter-plus-noise content, and a sparse matrix, which aims at detecting the targets. These methods showed that a matrix solution based on RPCA could be an efficient strategy to detect military targets and have advantages in terms of run-time processing compared with traditional methods, which usually is a pixel-by-pixel solution.

Matrix-based methods have a significant shortcoming when dealing with multidimensional data, which is ubiquitous in real applications. For example, an SAR image pair or stack is a 3-D object indexed by a temporal variable (number

Manuscript received 7 February 2024; revised 24 June 2024; accepted 17 July 2024. Date of publication 22 July 2024; date of current version 23 August 2024. This work was supported in part by the Brazilian National Council for Scientific and Technological Development (CNPq), in part by the Ministry of Science, Technology and Innovation (MCTI), in part by the Swedish-Brazilian Research and Innovation Centre (CISB), in part by Saab AB, in part by the Coordination for the Improvement of Higher Education Personnel (CAPES) (Pró-Defesa IV), and in part by São Paulo Research Foundation (FAPESP) (BI0S—Brazilian Institute of Data Science) under Grant 2020/09838-0. *(Corresponding author: Lucas P. Ramos.)*

Lucas P. Ramos is with the Department of Telecommunications, Aeronautics Institute of Technology, São José dos Campos 12228-900, Brazil, and also with the Department of Mathematics and Natural Sciences, Blekinge Institute of Technology, 371 79 Karlskrona, Sweden (e-mail: lucaspr@ita.br).

Dimas I. Alves and Renato Machado are with the Department of Telecommunications, Aeronautics Institute of Technology, São José dos Campos 12228-900, Brazil (e-mail: dimasirion@ita.br; rmachado@ita.br).

Leonardo T. Duarte is with the School of Applied Sciences, State University of Campinas, Limeira 13484-350, Brazil (e-mail: leonardo.duarte@fca.unicamp.br).

Mats I. Pettersson and Viet T. Vu are with the Department of Mathematics and Natural Sciences, Blekinge Institute of Technology, 371 79 Karlskrona, Sweden (e-mail: mats.pettersson@bth.se; viet.thuy.vu@bth.se).

Patrik Dammert is with Saab Surveillance, Saab AB, 412 89 Gothenburg, Sweden (e-mail: patrik.dammert@saabgroup.com).

Digital Object Identifier 10.1109/LGRS.2024.3431683

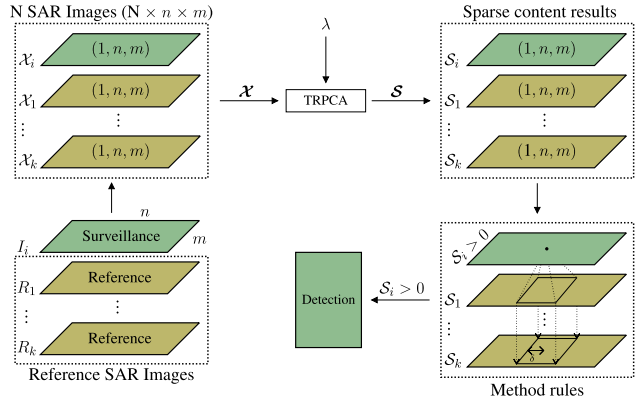

Fig. 1. CD scheme based on tensor robust PCA.

of images) and two spatial variables (rows and columns). Applying RPCA requires organizing the data into a matrix, ignoring the information embedded in the multidimensional structure that may be associated with targets or clutter-plus-noise content in SAR images [15]. An efficient way to face this issue is to extend the RPCA problem from matrices (i.e., 2-D) to tensors (i.e., 3-D), capturing the multifactor structure of the data [16], [17]. Recently, tensor RPCA (TRPCA) with a new tensor nuclear norm (TNN) was developed [18]. This approach, based on the tensor–tensor product (t-product) and tensor singular value decomposition (t-SVD), showed that TRPCA could exactly recover the low-rank and sparse tensor from its sum and outperform the RPCA problem [13], [18].

Motivated by the possible gains associated with SAR image stacks in CD methods and new technological advances in robust computer vision techniques, a CD method in VHF WR SAR image stacks based on TRPCA (CD-TRPCA) is proposed. The proposed CD-TRPCA is based on TRPCA via new TNN [18] and aims at exploring the spatial and temporal information in SAR image stacks on target detection applications. Furthermore, with the increase in the database of SAR systems, CD methods based on techniques that work with a larger number of images, such as TRPCA, are increasingly important. We use 24 VHF WR SAR images provided in [19] from the coherent all radio band sensing (CARABAS) II SAR system. It operates in the 20–90-MHz band and provides imagery with a spatial resolution of about 2.5 m.

Therefore, the main contribution of the work is to propose a CD method for WR SAR image stacks based on TRPCA, exploring the multidimensional diversity of the SAR image stack. Experiments on different stack configurations demonstrate that CD-TRPCA achieves competitive performance in comparison to state-of-the-art CD methods, allowing the use of different amounts of SAR images with the proposed method.

This letter is organized as follows. Section II presents the formulation of the TRPCA. The WR SAR CD method is introduced in Section III. In Section IV, the results and experimental aspects of the proposed method are presented and discussed. Finally, the conclusions are drawn in Section V.

II. Tensor Robust PCA

TRPCA is a tensor extension of RPCA, which in turn can be seen as a robust extension of classical PCA. However, both RPCA and PCA have limitations when dealing with high-dimensional data, as both the methods must first restructure the multidimensional data into a matrix, i.e., they ignore the information embedded in the multidimensional structure, causing a performance degradation [20].

TRPCA assumes that $\boldsymbol{\mathcal{X}} \in \mathbb{R}^{n_1 \times n_2 \times n_3}$ can be decomposed into a low-rank tensor $\boldsymbol{\mathcal{L}}_0 \in \mathbb{R}^{n_1 \times n_2 \times n_3}$ and a sparse tensor $\boldsymbol{\mathcal{S}}_0 \in \mathbb{R}^{n_1 \times n_2 \times n_3}$, satisfying $\boldsymbol{\mathcal{X}} = \boldsymbol{\mathcal{L}}_0 + \boldsymbol{\mathcal{S}}_0$, where n_1, n_2, and n_3 represent the horizontal, lateral, and frontal slices of the tensor, respectively. The problem of recovering $\boldsymbol{\mathcal{L}}_0$ and $\boldsymbol{\mathcal{S}}_0$ separately can be formulated by the following convex optimization problem:

$$\begin{aligned} &\text{minimize} \ \ \|\boldsymbol{\mathcal{L}}\|_* + \lambda \|\boldsymbol{\mathcal{S}}\|_1 \\ &\text{s.t.} \ \ \boldsymbol{\mathcal{L}} + \boldsymbol{\mathcal{S}} = \boldsymbol{\mathcal{X}} \end{aligned} \tag{1}$$

where $\|\cdot\|_1$ represents the l_1-norm and it is computed by the sum of all entries in $\boldsymbol{\mathcal{S}}$, i.e., $\|\boldsymbol{\mathcal{S}}\|_1 = \sum_{abc} |\boldsymbol{\mathcal{S}}_{abc}|$ and $\|\cdot\|_*$ represents the TNN [21], [22], and it is computed by the sum of singular values of all frontal slices of $\boldsymbol{\mathcal{L}}$, i.e.,$\|\boldsymbol{\mathcal{L}}\|_* := \sum_{t=1}^{n_3} \|\overline{\mathbf{L}}^{(t)}\|_*$, where $\overline{\mathbf{L}}^{(t)}$ is the tth frontal slice of $\overline{\boldsymbol{\mathcal{L}}}$, and $\overline{\boldsymbol{\mathcal{L}}} = \text{fft}(\boldsymbol{\mathcal{L}}, [], 3)$ is the discrete Fourier transformation (DFT) along the third dimension using the MATLAB command [18]. Note that the DFT is performed on all the tubes of $\boldsymbol{\mathcal{L}}$ since the tube of a tensor $\boldsymbol{\mathcal{A}} \in \mathbb{R}^{n_1 \times n_2 \times n_3}$ is denoted as $\boldsymbol{\mathcal{A}}(a, b, :)$, i.e., a vector derived by keeping the entries a and b fixed in a tensor [18].

This convex optimization problem aims at recovering a tensor of low tubal rank based on the TNN induced by the recent definition of the t-product and t-SVD [21], [23]. The tensor tubal rank is defined as the number of nonzero singular tubes of $\boldsymbol{\mathcal{D}}$, with $\boldsymbol{\mathcal{D}}$ being the f-diagonal tensor obtained from the t-SVD of a tensor $\boldsymbol{\mathcal{A}} = \boldsymbol{\mathcal{U}} * \boldsymbol{\mathcal{D}} * \boldsymbol{\mathcal{V}}^*$. The term "$f$-diagonal" is used when each frontal slice is diagonal [23]. The t-product is analogous to the matrix multiplication except that the circular convolution replaces the multiplication operation between the elements [18]. In the Fourier domain, circular convolution means a multiplication operation between the elements. Thus, the t-SVD can be easily calculated by solving several SVDs [23]. If the tensor tubal rank of $\boldsymbol{\mathcal{L}}_0$ is not too large and $\boldsymbol{\mathcal{S}}_0$ is reasonably sparse, Lu et al. [18] show that $\boldsymbol{\mathcal{L}}_0$ and $\boldsymbol{\mathcal{S}}_0$ are perfectly recovery by defining λ as

$$\lambda = \frac{1}{\sqrt{\max(n_1, n_2) n_3}}. \tag{2}$$

Different approaches for solving (1) exist. In this study, we considered the alternating direction method of multiplier (ADMM) framework, widely used to solve RPCA and its related problems [14], [18]. ADMM breaks the optimization problem into smaller pieces, each easier to handle [24]. For TRPCA, $\boldsymbol{\mathcal{L}}$ and $\boldsymbol{\mathcal{S}}$ are obtained alternatively with closed solutions and then updated. The complexity of the TRPCA solved by ADDM is equal to $\mathcal{O}(n_1 n_2 n_3 \log n_3 + n_1 n_2^2 n_3)$. Details on ADMM solving TRPCA can be found in [21] and [18].

III. Change Detection

The methodology of the proposed CD method is presented in Fig. 1. Let us consider a surveillance image I_i of size

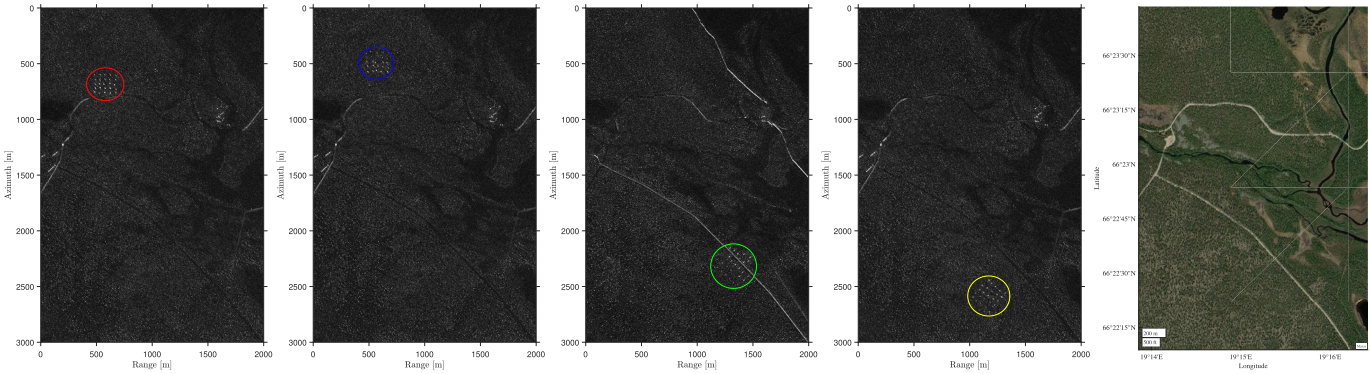

(a) (b) (c) (d) (e)

Fig. 2. Scattering magnitude of the ground scene from the CARABAS-II system with different target deployments (i.e., missions) and flight headings, and a map covering the same area as the SAR images. The circles show targets deployed in each mission. (a) Mission 2, Image 1 (225°). (b) Mission 3, Image 3 (225°). (c) Mission 4, Image 2 (135°). (d) Mission 5, Image 6 (230°). (e) Map of the region, June 2024.

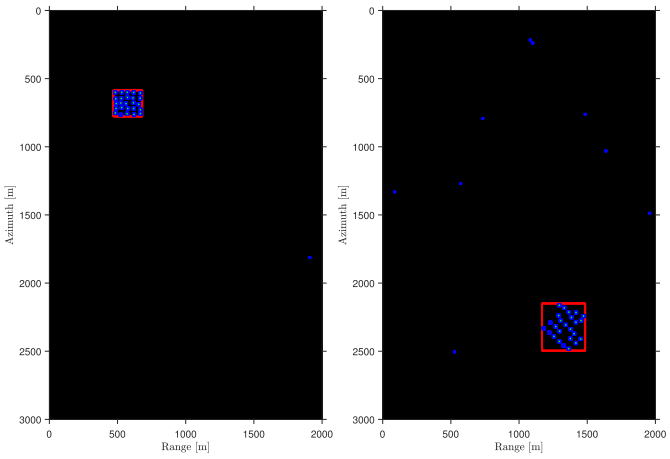

(a) (b)

Fig. 3. CD-TRPCA results for $\lambda = 2.8577 \times 10^{-3}$ and $N = 7$. (a) Mission 2, Image 1 [225°, Fig. 2(a)] as surveillance image and Mission 4 as reference. (b) Mission 4, Image 2 [135°, Fig. 2(c)] as surveillance image and Mission 2 as reference. The blue dots outside the red square mean FAs, while the ones inside the red square mean the known targets in the scene, i.e., ground truth, with green points as the detected targets.

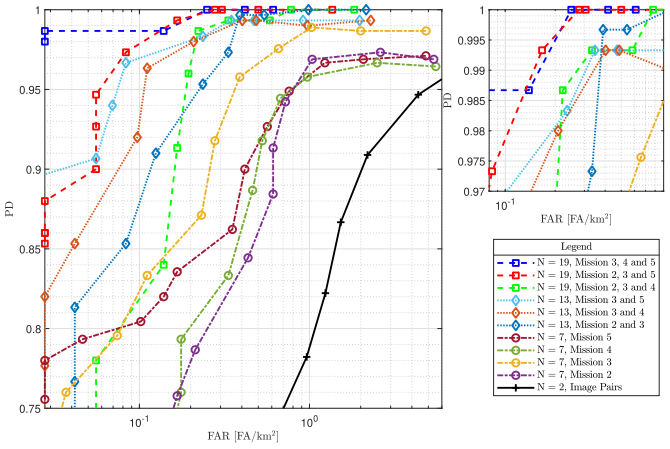

Fig. 4. ROC performance for the proposed method using different configurations of SAR images into the stack.

$n \times m$ (rows $\times$ columns), in which we aim to identify targets. For this, we consider a stack of k SAR images of size $n \times m$ $(R_1, R_2, \ldots, R_k)$ acquired in the same geographical area but at different time instants acting as a background representation and therefore are called reference images.

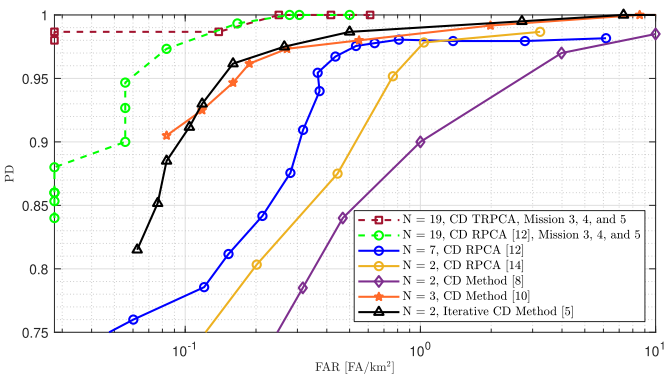

Fig. 5. ROC performance for the proposed and reference methods.

There are different combinations to form the tensor $\boldsymbol{\mathcal{X}}$. They differ in the way t-SVD is obtained. As we are proposing a CD method to exploit temporal and spatial information in the decomposition, $\boldsymbol{\mathcal{X}}$ is given by $N \times n \times m$, where N is the total number of SAR images in the stack given by $1 + k$, where k is the total number of reference images. Our approach allows the t-SVD to consider a temporal and spatial dimension, i.e., N and n, respectively. This is justified by the t-product definition [23], in which a size tensor is written as $n_1 \times n_2$ matrix of n_3 tubes, i.e., $N \times n$ matrix of m tubes. We evaluated other combinations, exploring both the temporal and spatial dimensions. However, there were no significant changes in performance.

$\boldsymbol{\mathcal{X}}$ is then decomposed into $\boldsymbol{\mathcal{L}}$ and $\boldsymbol{\mathcal{S}}$, where $\boldsymbol{\mathcal{L}}$ represents the low-rank subspace that can gradually change over time as is the background of $\boldsymbol{\mathcal{X}}$, and $\boldsymbol{\mathcal{S}}$ represents the sparse content of $\boldsymbol{\mathcal{X}}$, i.e., targets of $\boldsymbol{\mathcal{X}}$, which is of interest to our study. $\boldsymbol{\mathcal{S}}$ is formed with the sparse content of the surveillance image $(\mathcal{S}_i)$ and with the sparse content of the reference images $(\mathcal{S}_1, \mathcal{S}_2, \ldots, \mathcal{S}_k)$. Some method rules were adopted to explore the sparse information of the reference images and improve the detection in $\mathcal{S}_i$. These rules, which are presented below, were proposed by Ramos et al. [12] and proved very effective for CD applications focusing on target detection.

1) Only detections in $\mathcal{S}_i$ are counted. This rule is justified since we want to detect targets in surveillance images.
2) Only positive detection in $\mathcal{S}_i$ is counted. In the CD method, we look for variations that emerged in the

surveillance image (i.e., variations that do not appear in the reference images). These variations are mirrored in the sparse content of the surveillance image, i.e., $\mathcal{S}_i$ with positive values. However, we cannot rule out that reference images may have reflections referring to static objects in the same position (e.g., buildings, fences, and others). The absence of these structures only in the surveillance image is interpreted by the TRPCA as sparse content and separated into $\mathcal{S}_i$ with a negative value. For example, the CARABAS-II data are characterized by having targets in all SAR images. Then, if one considers reference images from the same deployment (i.e., targets in the same position), the TRPCA mirrors the targets of the reference images in $\mathcal{S}_i$ with negative values. Since these negative values represent reference content, such values can be discarded.

3) Detections in $\mathcal{S}_i$ which also occur, at least, in one of the reference images of the output sparse stack $(\mathcal{S}_1, \mathcal{S}_2, \ldots, \mathcal{S}_k)$ are discarded if they occur within a specified square window of $2\delta \times 2\delta$ pixels. The idea of this rule is to eliminate possible detection related to the same object in the surveillance and any reference image. Based on the spatial resolution of the CARABAS-II system, Ramos et al. [12] showed that $\delta = 9$ pixels could further improve the performance of the RPCA-based CD method. We adopted this same radius for comparison purposes.

IV. Experimental Results

A. Dataset

We used 24-magnitude SAR images (calibrated and coregistered) from the CARABAS-II system in the strip map SAR mode operating at 20–85 MHz, HH-polarization, and an incidence angle of 58°. These images are available for the VHF WR SAR CD research as a challenging problem [9]. Each magnitude image of 3000×2000 covers the same ground area as 6 km^2 (3×2 km) and contains 25 military vehicles of different dimensions as testing targets (length, width, height): ten TGB11 (4.4, 1.9, 2.2 m), eight TGB30 (6.8, 2.5, 3 m), and seven TGB40 (7.8, 2.5, 3 m). In addition, the region is characterized by forests, power lines, lakes, roads, buildings, fields, and fences [9].

The images are divided into four missions: Missions 2–5, where each mission represents a different target deployment. Each mission consists of six images collected under three different flight headings: 2 of 225° (Images 1 and 3), 2 of 135° (Images 2 and 4), and 2 of 230° (Images 5 and 6). Fig. 2 shows scattering magnitude SAR images of the ground scene with the targets deployed in each mission, considering images acquired from different flight headings.

B. Implementation Aspects

The experimental evaluation was performed using all 24 VHF WR SAR images and considering the processing scheme provided in Fig. 1. The method proposed herein uses the TRPCA implementation presented in [25]. Thus, the TRPCA implementation parameters were the same as for [18] and [25], such as initialization parameters, step length for convergence, and stopping criteria.

Each 3000×2000 SAR image is organized into a third-order tensor given by $1 \times 3000 \times 2000$. Thus, $\boldsymbol{\mathcal{X}}$ is formed by $N \times 3000 \times 2000$. According to [18], a value of λ that exactly recovers $\boldsymbol{\mathcal{L}}_0$ and $\boldsymbol{\mathcal{S}}_0$ under certain assumptions can be theoretically obtained by (2). Based on $\boldsymbol{\mathcal{X}} \in \mathbb{R}^{N \times 3000 \times 2000}$ and $3000 \gg N$, we have $\lambda = ((\max(n_1, n_2)n_3)^{1/2})^{-1} = ((3000 \times 2000)^{1/2})^{-1} = 4.0825 \times 10^{-4}$ for the CARABAS-II dataset. This value is the same obtained in RPCA-based CD methods [12], [14]. These methods empirically showed that better results can be obtained when working with a λ approximately nine times larger. Thus, we analyzed our method in a range of 3–13× the value of 4.0825×10^{-4} with a 0.5 step size.

C. Discussion

The proposed method is evaluated based on the probability of detection (PD), defined by the ratio between the number of targets detected in the surveillance image and the known number of targets in the surveillance image, i.e., 25 targets. The false alarm rate (FAR) is also considered and is calculated from the ratio between the number of FAs detected and the area under surveillance, i.e., 6 km^2.

Aiming to illustrate a result obtained using the CD proposed method, Fig. 3 presents the detection results for $\lambda = 2.8577 \times 10^{-3}$ and $N = 7$. In Fig. 3(a), one can observe Image 1 from Mission 2 as a surveillance image and six images from Mission 4 as reference images. In Fig. 3(b), we have Image 4 from Mission 4 as a surveillance image and six images from Mission 2 as reference images. Note that depending on the surveillance SAR image and the reference images used in the stack, one may have a result of PD = 0.960 and FAR = 0.167 FA/km^2 [Fig. 3(a)] or a result of PD = 0.840 and FAR = 1.500 FA/km^2 [Fig. 3(b)]. If we compare both the surveillance images used for the results presented in Fig. 3 [i.e., Fig. 2(a) and (c)], it is possible to observe that the difference in FAR is mainly related to elongated structures sensitive to flight heading, which increase the number of FAs. Furthermore, it is visually observed that some targets in Fig. 2(c) present a weaker backscatter than those in Fig. 2(a), which may justify a loss in detection.

Fig. 4 shows the method's overall performance in receiver operating characteristic (ROC) curves, obtained by varying the λ value. Our approach is evaluated considering different missions as a reference and also different N stack sizes. The PD and FAR values for each λ in the ROC curves using SAR image stacks were obtained from the average of the $(24 - k)$ surveillance images. The higher the number k of reference images considered, the fewer surveillance images will be considered on average. The image pairs' curve in Fig. 4 used the same image pairs of [9] and [14].

Initially, we analyzed our method with only one mission (six images) as a reference, i.e., $N = 7$ and $k = 6$. In this analysis, similar to [12], the best ROC curve was obtained when using Mission 3 as a reference, while a standard behavior was presented in the other missions. Mission 3 targets have weaker backscatter when compared with targets in other missions,

which generally reduces the performance of CD methods. However, when considering this mission as a reference, we are removing such images as surveillance images, and therefore, better performance is obtained. For this analysis, it was possible to get an FAR $= 0.657$ FA/km^2 and a PD $= 0.976$ using $\lambda = 26.536 \times 10^{-4}$ and Mission 3 as a reference. Since Mission 3 as reference yielded the highest performance, it has been selected and fixed for the remaining experiments.

We expanded our analysis using two and three missions as a reference, respectively, $N = 13$ and $N = 19$. Our method shows that the best ROC curves are obtained with more SAR images in the stack, i.e., $N = 19$. This analysis shows that the increase in temporal diversity, i.e., the increase in N, provides more a priori information for the TRPCA about the clutter and the target, and consequently, better performance is obtained. In this analysis, we have our best case with an FAR $= 0.028$ FA/km^2 and a PD $= 0.987$ using $\lambda = 26.536 \times 10^{-4}$ and Missions 3–5 as reference.

Fig. 5 shows comparison of our best ROC curve with other best ROC curves from other CD methods on VHF WR SAR images. For this, we considered the proposed CD methods based on matrix RPCA [12], [14], a recent iterative CD method [5], and one of the first CD methods on VHF WR SAR images pairs [8] and stacks [10]. For a fair comparison, we expanded [12] to our best case. Note that the proposed method in the present work provides clear gains in performance compared with previous approaches, which are based on either image pairs or stacks.

V. Conclusion

This letter proposed a CD method based on TRPCA for WR SAR image stacks. The proposed approach benefits from the multidimensional characteristics of TRPCA, obtaining accurate information on the data and consequently reducing FAs. Stacks with seven, 13, and 19 were considered for the experiments. The best results were obtained when more reference images were added to the stack, i.e., when more reference information was provided to TRPCA. Experiments on the CARABAS-II dataset show that the proposed method overcomes state-of-the-art CD methods, such as the one based on the matrix robust PCA, in terms of the PD and FAR on the same dataset. In particular, our method achieves a PD of 99% and an FAR $= 0.028$ FA/km^2. In recent years, there has been a tremendous increase in the release of SAR systems, which has allowed for greater accessibility to different types of SAR images. Thus, CD methods that enable the exploration of temporal and spatial diversity in SAR image stacks, such as TRPCA, become even more important.

References

[1] L. Khelifi and M. Mignotte, "Deep learning for change detection in remote sensing images: Comprehensive review and meta-analysis," *IEEE Access*, vol. 8, pp. 126385–126400, 2020.

[2] Y. Afaq and A. Manocha, "Analysis on change detection techniques for remote sensing applications: A review," *Ecolog. Informat.*, vol. 63, Jul. 2021, Art. no. 101310.

[3] A. Moreira, P. Prats-Iraola, M. Younis, G. Krieger, I. Hajnsek, and K. P. Papathanassiou, "A tutorial on synthetic aperture radar," *IEEE Geosci. Remote Sens. Mag.*, vol. 1, no. 1, pp. 6–43, Mar. 2013.

[4] W. Ye, C. Paulson, and D. Wu, "Target detection for very high-frequency synthetic aperture radar ground surveillance," *IET Comput. Vis.*, vol. 6, no. 2, pp. 101–110, 2012.

[5] D. I. Alves et al., "Change detection method for wavelength-resolution SAR images based on Bayes' theorem: An iterative approach," *IEEE Access*, vol. 11, pp. 84734–84743, 2023.

[6] Z. Xu, "Wavelength-resolution SAR speckle model," *IEEE Geosci. Remote Sens. Lett.*, vol. 19, pp. 1–5, 2022.

[7] R. Machado, V. T. Vu, M. I. Pettersson, P. Dammert, and H. Hellsten, "The stability of UWB low-frequency SAR images," *IEEE Geosci. Remote Sens. Lett.*, vol. 13, no. 8, pp. 1114–1118, Aug. 2016.

[8] L. M. H. Ulander, M. Lundberg, W. Pierson, and A. Gustavsson, "Change detection for low-frequency SAR ground surveillance," *Proc. IEEE Radar, Sonar Navigat.*, vol. 152, no. 6, pp. 413–420, 2005.

[9] M. Lundberg, L. M. Ulander, W. E. Pierson, and A. Gustavsson, "A challenge problem for detection of targets in foliage," *Proc. SPIE*, vol. 6237, pp. 160–171, Apr. 2006.

[10] V. T. Vu, "Wavelength-resolution SAR incoherent change detection based on image stack," *IEEE Geosci. Remote Sens. Lett.*, vol. 14, no. 7, pp. 1012–1016, Jul. 2017.

[11] B. G. Palm et al., "Wavelength-resolution SAR ground scene prediction based on image stack," *Sensors*, vol. 20, no. 7, p. 2008, Apr. 2020.

[12] L. P. Ramos et al., "A wavelength-resolution SAR change detection method based on image stack through robust principal component analysis," *Remote Sens.*, vol. 13, no. 5, p. 833, Feb. 2021.

[13] E. Candès, X. Li, Y. Ma, and J. Wright, "Robust principal component analysis?" *J. ACM*, vol. 58, no. 3, pp. 1–37, 2011.

[14] C. Schwartz et al., "Change detection in UWB SAR images based on robust principal component analysis," *Remote Sens.*, vol. 12, no. 12, p. 1916, Jun. 2020.

[15] Q. Gao, P. Zhang, W. Xia, D. Xie, X. Gao, and D. Tao, "Enhanced tensor RPCA and its application," *IEEE Trans. Pattern Anal. Mach. Intell.*, vol. 43, no. 6, pp. 2133–2140, Jun. 2021.

[16] A. Cichocki et al., "Tensor decompositions for signal processing applications: From two-way to multiway component analysis," *IEEE Signal Process. Mag.*, vol. 32, no. 2, pp. 145–163, Mar. 2015.

[17] N. D. Sidiropoulos, L. De Lathauwer, X. Fu, K. Huang, E. E. Papalexakis, and C. Faloutsos, "Tensor decomposition for signal processing and machine learning," *IEEE Trans. Signal Process.*, vol. 65, no. 13, pp. 3551–3582, Jul. 2017.

[18] C. Lu, J. Feng, Y. Chen, W. Liu, Z. Lin, and S. Yan, "Tensor robust principal component analysis with a new tensor nuclear norm," *IEEE Trans. Pattern Anal. Mach. Intell.*, vol. 42, no. 4, pp. 925–938, Apr. 2020.

[19] U.S. Air Force. *The Sensor Data Manage System* Accessed: May 3, 2023. [Online]. Available: https://www.sdms.afrl.af.mil

[20] X. Xu, R. Gao, Y. Qing, J. Feng, Z. Zeng, and M. Wang, "Hyperspectral image mixed noise removal via tensor robust principal component analysis with tensor-ring decomposition," *Int. J. Remote Sens.*, vol. 44, no. 5, pp. 1556–1578, Mar. 2023.

[21] C. Lu, J. Feng, Y. Chen, W. Liu, Z. Lin, and S. Yan, "Tensor robust principal component analysis: Exact recovery of corrupted low-rank tensors via convex optimization," in *Proc. IEEE Conf. Comput. Vis. Pattern Recognit. (CVPR)*, Jun. 2016, pp. 5249–5257.

[22] Y.-B. Zheng, T.-Z. Huang, X.-L. Zhao, T.-X. Jiang, T.-Y. Ji, and T.-H. Ma, "Tensor N-tubal rank and its convex relaxation for low-rank tensor recovery," *Inf. Sci.*, vol. 532, pp. 170–189, Sep. 2020.

[23] M. E. Kilmer and C. D. Martin, "Factorization strategies for third-order tensors," *Linear Algebra Appl.*, vol. 435, no. 3, pp. 641–658, Aug. 2011.

[24] S. Boyd, N. Parikh, E. Chu, B. Peleato, and J. Eckstein, "Distributed optimization and statistical learning via the alternating direction method of multipliers," *Found. Trends Mach. Learn.*, vol. 3, no. 1, pp. 1–122, 2010.

[25] C. Lu. (2023). *Tensor Robust PCA*. Accessed: Aug. 3, 2023. [Online]. Available: https://github.com/canyilu/Tensor-Robust-Principal-Component-Analysis-TRPCA